Article:
Kumagai, S, Alvarez, J, Blanco, PH et al. (4 more authors) (2015) Novel Ni-Mg-Al-Ca catalyst for enhanced hydrogen production for the pyrolysis-gasification of a biomass/plastic mixture. Journal of Analytical and Applied Pyrolysis, 113. 15 - 21. ISSN 0165-2370

https://doi.org/10.1016/j.jaap.2014.09.012

Novel Ni-Mg-Al-Ca catalyst for enhanced hydrogen production for the pyrolysis-gasification of a biomass/plastic mixture

Shogo Kumagai,[a,b] Jon Alvarez,[c] Paula H. Blanco,[d] Chunfei Wu,[d] Toshiaki Yoshioka,[a] Martin Olazar,[c] Paul T. Williams [d,*]

[a] Graduate School of Environmental Studies, Tohoku University, 6-6-07 Aoba, Aramaki-aza, Aoba-ku, Sendai, Miyagi 980-8579, Japan

[b] Japan Society for the Promotion of Science, 8 Ichibancho, Chiyoda-ku, Tokyo 102-8472, Japan

[c] Department of Chemical Engineering, University of the Basque Country, P.O. Box 644, E-48080, Bilbao, Spain

[d] Energy Research Institute, University of Leeds, Leeds LS2 9JT, UK

Abstract: A Ni-Mg-Al-Ca catalyst was prepared by a co-precipitation method for hydrogen production from polymeric materials. The prepared catalyst was designed for both the steam cracking of hydrocarbons and for the in situ absorption of CO_2 via enhancement of the water-gas shift reaction. The influence of Ca content in the catalyst and catalyst calcination temperature in relation to the pyrolysis-gasification of a wood sawdust /polypropylene mixture was investigated. The highest hydrogen yield of 39.6 mol H_2/g Ni with H_2/CO ratio of 1.90 was obtained in the presence of the Ca containing catalyst of molar ratio Ni:Mg:Al:Ca = 1:1:1:4, calcined at 500 °C. In addition, thermogravimetric and morphology analyses of the reacted catalysts revealed that Ca introduction into the Ni-Mg-Al catalyst prevented the deposition of filamentous carbon on the catalyst surface. Furthermore, all metals were well dispersed in the catalyst after the pyrolysis-gasification process with 20-30 nm of NiO sized particles observed after the gasification without significant aggregation.

Keywords: Pyrolysis; Gasification; Hydrogen; Biomass; Plastic; Nickel catalyst

(for correspondence; p.t.williams@leeds.ac.uk; Tel: +44 113432504; Fax: +44 1132467310)

1. Introduction

The continuous and increasing demand for fossil fuels [1] is primarily as a result of the growing wealth and increasing population in developing countries. However, concerns in relation to environmental issues such as energy supply shortage, resource depletion, and global warming, make it necessary to consider the development of renewable energy instead of fossil fuels.

Hydrogen is one of the key clean energy carriers, which can be used for hydrogen engine and hydrogen-fuel cells since it only generates water on combustion. In addition, hydrogen is necessary for the petroleum industry as petrochemical feedstock and for steel plants as a reduction agent. Currently, the large majority of hydrogen is produced from fossil fuel sources. Hydrogen production from renewable resources such as biomass is an attractive potential technology option since it is large available resource and is carbon neutral [2]. Waste plastics are also a potential hydrogen feedstock since plastics are generated in large quantities [3], and are mainly produced from fossil fuels. Hydrogen production from the co-processing of biomass and plastics is therefore an interesting topic of research.

Thermal processing has been applied to produce hydrogen from biomass [4-6] and waste plastics [7-10]. However, the yield of hydrogen from biomass is typically low, therefore, addition of plastics which have a high hydrogen content into the biomass feedstock would enhance the amount of hydrogen in the gaseous product stream. Co-pyrolysis for hydrogen production was reported with various biomass-plastic combinations, such as wood-polypropylene [11], pine cone-polypropylene, pine cone-polyethylene, and pine cone–polystyrene [12], and pubescens-low density polyethylene [13]. These investigations were carried out using various reactors such as a fixed-bed reactor, fluidized-bed reactor, spouted-bed reactor, screw kiln reactor, and molten

carbonate reactor, however, which are often combined with catalysts in order to improve the hydrogen production.

Many types of catalysts such as alkali and alkali earth metal compounds [14-16], Fe [17], Rh [18], and Ru [19] supported catalysts have been investigated for biomass and plastic gasification. However, nickel based catalysts have been commonly used with steam as the hydrogen production catalyst. Czernik and French [20] investigated the gasification of polypropylene using C11-NK (commercial nickel catalyst), recovering 80% hydrogen of the theoretical potential of polypropylene. Liu et al. [13] and Ruoppolo et al. [21] carried out the co-gasification of biomass/plastic mixtures using Ni loaded γ-Al_2O_3 and, Ni and Pd loaded Al-MCM-41(mesoporous aluminosilicates), respectively, which also promoted hydrogen production.

Our previous work has investigated separately hydrogen production from biomass and plastics using various types of Ni catalysts. Wu et al. [22] investigated polypropylene gasification using Ni-Al and Ni-Mg-Al catalysts synthesized by a co-precipitation method [23], which showed that the introduction of Mg into the Ni-Al catalyst significantly decreased the coke formation on the catalyst surface without hydrogen yield loss. The Ni-Mg-Al catalyst was also applied to the gasification of biomass components such as cellulose, xylan, and lignin, resulting in the highest gas yield of 73.0 wt% from cellulose at 800 ºC [24]. Furthermore, a Ni-Mg-Al-CaO catalyst synthesized by the calcination of a mixture of Ni-Mg-Al catalyst and calcium oxide (CaO) was used as a catalyst for gasification and in situ CO_2 absorption [25,26]. As is well known, the water-gas shift reaction is an equilibrium reaction as;

$$CO + H_2O \rightleftarrows CO_2 + H_2 \qquad (1)$$

CaO is a common CO_2 absorbent, which can be used repeatedly by the cycle of carbonation/decarbonation [27,28]. That reaction is described as

$$CaO + CO_2 \rightleftarrows CaCO_3 \qquad (2)$$

The stability of CO_2 absorption for the Ni-Mg-Al-CaO catalyst was improved in comparison to only CaO, and the H_2/CO ratio in the gaseous products was increased with the CaO addition [25]. Therefore, it was suggested that the water-gas shift reaction was enhanced by the CaO addition due to the in-situ CO_2 absorption. However, further studies for the Ni-Mg-Al-CaO catalyst system are needed to optimize the configuration of the catalyst in terms of hydrogen production and catalyst stability.

In this work, we further investigate Ni-Mg-Al-Ca catalysts with different Ca content and calcination temperature. The developed catalysts were characterized for physical and chemical properties, and tested for hydrogen production from the pyrolysis-gasification of a wood sawdust/polypropylene mixture.

2. Experimental

2.1 Materials

Wood sawdust, with a particle size of less than 0.2 mm, was used in the experiments as a representative biomass sample. Carbon, hydrogen, nitrogen, and sulfur content of the samples was determined using a Carlo Erba Flash EA 1112 elemental analyser, while the oxygen content was determined by difference (Table 1). A Shimadzu TGA-50H analyser was used to perform the proximate analysis of the wood sample (N_2 atmosphere, room temp. → 25 °C min^{-1} → 110 °C (10 min) → 925 °C). Moisture and volatile contents corresponded to the weight loss until 110 °C, and between 110 °C and 925 °C, respectively. The fixed carbon content was determined by the introduction of air which combusts the fixed carbon in the sample, leaving the ash residue. Polypropylene was obtained as 2.0 mm virgin polymer pellets provided by BP Chemicals, UK.

2.2 Catalyst Preparation

The Ni–Mg–Al-Ca catalyst was prepared by a co-precipitation method using the rising pH technique according to the method reported by Garcia et al. [23] The 1 M $NH_4(OH)$ as precipitant, was added to 200 ml of an aqueous solution containing $Ni(NO_3) \cdot 6H_2O$, $Mg(NO_3)_2 \cdot 6H_2O$, $Al(NO_3)_3 \cdot 9H_2O$, and $Ca(NO_3)_2 \cdot 4H_2O$. The precipitation was carried out at 40 °C with moderate stirring until a final pH of 8.3 was obtained and then filtered. The filter cake was dried at 105 °C overnight and then calcined at 500 °C and 750 °C for 3h with a heating rate of 10 °C min^{-1} in air atmosphere. Preparaton conditions of catalysts and catalyst abbreviations are summarized in Table 2.

2.3 Pyrolysis-Gasification Experiments

The pyrolysis-gasification experiments on the mixture of wood sadust and polypropylene were carried out in a two-stage stainless tube reactor, placed in two independently heated electric furnaces (Figure 1). The pyrolysis was carried out in the first stage and the evolved volatiles were passed directly to the second stage reactor where steam gasification of the pyrolysis gases took place in the presence of the different catalysts. A sample holder filled with 2.0 g of sample, containing 1.5 g of wood sawdust and 0.5 g of polypropylene (weight ratio of wood sawdust/polyproylene = 4.0) was placed in the pyrolysis first stage. The gasification reactor was maintained at 800 °C under a constant N_2 flow of 80 mL min^{-1}. This temperature is enough to decarbonate $CaCO_3$ into CaO [26]. When constant temperature conditions were achieved in the

catalyst gasification reactor, the pyrolysis reactor was heated up at 40 °C min^{-1} from ambient temperature to 600 °C and held at that temperature for 30 minutes, in addition, water was fed into the gasification reactor via a syring pump at the feeding rate of 0.05 g min^{-1} to generate steam. The produced pyrolysis gases were carried by the N_2 flow into the gasification reactor, where reaction with steam in the presence of the catalyst occurred. Oil and unreacted water were collected in the condensation system consisting of glass condensers cooled by air and dry ice. Non-condensed gases were collected in a Tedlar™ gas sample bag, which were analysed by gas chromatography (GC). The amounts of injected water, condensed liquid, and char were calculated by weighing the syringe, the condensers, and the sample holder before and after the experiments. Experiments were repeated to ensure the reliability of the results.

Gaseous products collected in the Tedlar™ gas sample bag were analyzed using GC (Varian 3380GC) equipped with a thermal conductivity detector (GC-TCD) and a flame ionization detector (GC-FID). H_2, CO, O_2, and N_2 were analyzed using a GC-TCD (Packed-column:molecular sieve (60~80 mesh size)). CO_2 was quantified using a GC-TCD (Packed-column:Hysep packing material (80~100 mesh size)). Hydrocarbons (C1-C4) were analyzed by a GC-FID (Packed-column:Hysep packing material (80~100 mesh size)).

2.4 Characterisation of Reacted Catalysts

The reacted catalysts from the pyrolysis-gasification experiments, were analysed by temperature-programmed oxidation (TPO) using a Stanton-Redcroft analyser. About 20 mg of each sample was weighed and placed in a crucible; once the equipment was equilibrated the sample was heated up to 800 ºC under air atmosphere with 15 ºC min^{-1} as heating rate and 10 min

of dwell time. Furthermore, reacted catalysts were investigated by thermogravimetric analyser (TGA) interfaced with a Nicolet Magna IR-560 (FTIR) under air atmosphere.

A SEM LEO 1530 high-resolution scanning electron microscope was used to characterise and examine the surface morphology of the fresh and reacted catalysts. The catalysts were also examined by transmission electron microscopy (TEM) using a Phillips CM200 equipped with energy dispersive X-ray spectroscopy (EDX). The micrographs at different magnifications were obtained. Elemental mapping was also obtained for selected elements.

3. Results and Discussion

3.1 Influence of the Ca content and Calcination Temperature on the Gas Yields

The decomposition products from the pyrolysis-gasification experiments were classified into three groups: (1) gases, which did not condense in the cooling traps; (2) liquids, which were condensable in the condensers including water and hydrocarbon compounds; and (3) char, which remaind in the sample holder. The obtained mass balances are summarized in Table 3. Product yields were standardized on the basis of the total weight of sample and injected water, or only sample weight. Due to the reaction with steam, the mass balance was able to surpass 100 wt%.

In the absence of catalyst, gas and char yield, based on the sample weight, were 52.9 wt% and 17.2 wt%, respectively. Our previous work showed 40.7 wt% of gas and 33.5 w% of char from wood biomass gasification in the absence of catalyst [26], therefore the conversion rate and gas yield were improved by polypropylene addition. It might be due to the decrease of biomass components (cellulose, hemicellulose, and lignin) which are a cause for higher char production in the feedstock [5]. In contrast, gas yield was drastically increased in the presence of the 750-Ca0,

catalyst resulting in 96.9 wt% yield. At the same time, liquid yield was decreased with the increase of gas production since steam was consumed for gasification. The gas yield was decreased with the increase of Ca content since the gasification reaction (3) catalyzed by Ni was decreased due to the decrease of Ni content in the catalyst. The apparent influence of calcination temperature on the gas yield was not observed.

$$C_nH_mO_z + (n-z)H_2O \rightarrow nCO + (n - z + m/2)H_2 \qquad (3)$$

3.2 Influence of the Ca Content and Calcination Temperature on the Gas Composition

The hydrogen yields in relation to sample weight and nickel weight are shown in Figure 2. Hydrogen yield in relation to sample weight was drastically increased from 5.6 mmol H_2 g^{-1} sample in the absence of catalyst to 31.5 mmol H_2 g^{-1} sample in the presence of the 750-Ca0 catalyst since the reaction (3) was accelerated in the presence of Ni. However, the hydrogen yield was decreased with the increase of Ca content, resulting in 24.9 mmol H_2 g^{-1} sample in the presence of the 750-Ca4 catalyst, which was due to the decrease of Ni content which also resulted in a decrease of gas yield. In contrast, the hydrogen yield in relation to nickel weight was increased with the increase of Ca content in the catalyst, which suggets that production efficiency of hydrogen per mass of nickel was improved. Therefore, it further suggests that CaO in the catalyst was effective as an in situ CO_2 absorbent, enhancing the water-gas shift reaction (reaction (1)).

The influence of calcination temperature on the hydrogen yield was investigated in the presence of 750-Ca4 and 500-Ca4 catalysts (Figures 2 and 3), resulting in the highest hydrogen yield of 39.6 mol H_2 g^{-1} Ni using the 500-Ca4 catalyst. It has been reported that the higher

calcination temperature markedly accelerated the sintering of CaO [29], which decreased the CO_2 capture capacity [30]. Therefore, it was expected that the CO_2 capture capacity of the 500-Ca4 catalyst would be the highest in our prepared catalysts, enhancing the in situ CO_2 absorption. In addition, interaction between Ni and the catalyst support might be lower for the lower temperature calcination catalyst due to the lower sintering of the catalyst support, resulting in the highest hydrogen yield in the presence of the 500-Ca4 catalyst. Our previous work reported the influence of mixing CaO into a Ni-Mg-Al catalyst upon the gasification of wood biomass, which resulted in a maximum hydrogen yield in the presence of 20 wt% CaO content [26]. In the present work, the maximum hydrogen yield was obtained in the presence of the 500-Ca4 catalyst, which is characterized by a CaO content of 57 wt%. Further reduction of Ni content in the catalyst was achieved by introducing CaO into Ni-Mg-Al catalyst.

The gas composition and H_2/CO ratio are summarized in Figure 3. Hydrocarbons were produced from pyrolysis of the wood sawdust/polypropylene mixture, especially for polypropylene which preferentially produces more hydrocarbons [31]. However, hydrocarbons were markeldy decreased in the presence of the catalysts since the Ni accelerated the production of CO and H_2 from the pyrolysis volatiles (reaction 3). The gas composition was not affected by the difference of catalyst preparation conditions. Notably, CO_2 composition was not significantly changed because almost all CO_2 was released at the temperature of the experiments. The H_2/CO ratio was significantly increased in the presence of catalyst, which was slightly increased with the increase of Ca content in the catalyst. This behavior corresponded to our previous work using Ni-Mg-Al-CaO catalyst with biomass as feedstock [26].

The proposed reaction scheme for the gasification of the wood sawdust/polypropylene mixture using Ni-Mg-Al-Ca catalyst is summarized in Figure 4. Firstly, pyrolysis products of wood sawdust/polypropylene mixture are carried into the gasification reactor, where reaction

with steam in the presence of the Ni-Mg-Al-Ca catalysts occurrs. The NiO catalyzes the gasification of the biomass/plastic pyrolysis products consuming water and producing H_2, CO, CO_2, and other hydrocarbons (reaction (3)). Increase of the total gas yield with the increase of Ni content in the catalyst was due to this reaction. In addition, the reforming capacity of CaO might be significant if the CaO content increases in the catalyst [32]. The produced CO and H_2O derived from steam can be converted into H_2 and CO_2 by the water-gas shift reaction (reaction (1)), which was enhanced by the CO_2 absorption by CaO. The increase of the hydrogen yield in relation to Ni weight and H_2/CO ratio with the increase of Ca content and decrease of calcination temperature was due to this reaction. Therefore, CaO might take part in both the steam reforming and the CO_2 capture simultaneously.

3.3 Characterization of Reacted Catalysts

3.3.1 TGA-TPO and TGA-FTIR Analyses of the Reacted Catalysts

The reacted catalysts after the pyrolysis-gasification of the wood sawdust/polypropylene mixture were analyzed by TGA-TPO, and the results are shown in Figure 5. The weight loss observed at around 100 °C for all the catalysts was due to the release of moisture in the catalysts [26, 33]. The weight increase at ~300 °C corresponded to the oxidation of Ni which was produced from the reduction of NiO by the reduction agents such as H_2 and CO produced during the pyrolysis-gasification [24, 31, 34]. A lower Ni oxidation for the catalysts produced at the higher calcination temperature was observed, indicating the stronger interaction between Ni and the catalyst support. In contrast, the highest Ni oxidation was obtained with the 500-Ca4 catalyst, suggesting these results can be connected with the hydrogen production. The onset of the Ni

oxidation temperature of the Ca containing catalysts was higher than that of the non-Ca catalyst (750-Ca0), which was similar to our previous results obtained with a Ni-Mg-Al and CaO catalyst mixture [26]. Weight loss for TPO temperatures over 550 °C suggested two possibilities; one for the oxidation of filamentous carbon deposited on the catalyst surface [35, 36], and the another for the decarbonation of the $CaCO_3$ which was not decomposed during the gasification experiments.

An example TGA-FTIR spectrogram for the reacted 750-Ca4 catalyst is shown in Figure 6. The doubly degenerate bond (650 cm^{-1}) and asymmetric stretch (2650 cm^{-1}) of CO_2 were clearly observed from 600 °C, which increased with the temperature increase. Mackee [37] showed that decarbonation of $CaCO_3$ can start at around 580 °C in an air atmosphere, therefore, $CaCO_3$ which did not decompose during the gasification process was decarbonated. Notably, spectrum of water (1300 to 2000 cm^{-1} and 3500 to 4000 cm^{-1}) were observed at slightly higher temperature than CO_2 onset. Therefore, bulk $Ca(OH)_2$ covered by $CaCO_3$ might be dehydrated with the $CaCO_3$ decarbonation, which has not observed in our previous work using Ni-Mg-Al-CaO catalyst [26].

3.3.2 SEM Analysis of the Fresh and Reacted Catalysts

Morphologies of the fresh and reacted catalysts were investigated by SEM analysis, which are shown in Figure 7. Material was deposited on the fresh 750-Ca0 catalyst surface (Figure 7 (a)), however, which could not be observed on the Ca containing fresh catalysts (Figure 7 (c), (e), (g), and (h)). After the gasification, filamentous carbon was deposited on the 750-Ca0 catalyst surface (Figure 7 (b)). Wu et al. [24] reported that negligible amount of filamentous carbon was depositted on the Ni-Mg-Al surface during the pyrolysis-gasification of wood biomass [24]. On the other hand, filamentous carbon was observed when polypropylene was gasified using Ni-Mg-

Al catalyst [31], hence, the deposited filamentous carbon might be mainly derived from the polypropylene fraction in the feed material. Interestingly, filamentous carbon could not be found on the reacted Ca containing catalyst surface except for the 500-Ca2 catalyst (Figure 7 (d), (f), (h), and (j)), suggesting that introduction of Ca into the Ni-Mg-Al catalyst made it possible to reduce coke deposition on the catalyst surface. It also indicates that higher Ca content or higher calcination temperature is required to prevent the deposit of filamentous carbon on the catalyst surface. Remiro et al. [38] reported that the filamentous carbon grows by the reaction between active carbon precursors adsorbed on the catalyst surface. Therefore, the activity of the catalyst surface might be reduced by Ca introduction, resulting in negligible coke deposition on the catalyst surface. The surface morphology of the 750-Ca4 catalyst was changed after the pyrolysis-gasification reaction, suggesting sintering of CaO might be rapidly progressed at higher Ca content and higher calcination temperature.

3.3.3 TEM-EDX Analysis of the Reacted Catalysts

In order to investigate the nano-scale morphology of the reacted catalysts, the reacted 750-Ca2 and 500-Ca4 catalysts were analyzed by TEM (Figure 8). Dark-colored particles and can be observed in the images. The particle densities of the two reacted catalysts were different, it was expected that higher calcination temperature increased sintering of the catalyst. In addition, particles (NiO particles) observed in the 500-Ca4 catalyst were smaller (about 20-30 nm) and well dispersed compared with the 750-Ca2 catalyst. It was considered that lower Ni concentration and lower calcination temperature might prevent the sintering of NiO particles during the gasification process.

The TEM image, elemental mapping, and EDX spectra of the reacted 750-Ca2 catalyst are shown in Figure 9. Elemental mapping revealed that all metals were well dispersed in the catalyst after reaction, additionally, 20 to 30 nm sized NiO particles were clearly observed in TEM image and Ni mapping. Inaba et al. [39]. prepared various types of NiO supported zeolite for gasification of cellulose, which showed 10-20 nm particle size of NiO in the fresh catalysts. However, the NiO particles were sintered after the gasification, resulting in a particle size of about 100 nm. Therefore, the catalysts produced in this work with introduction of Ca might prevent the aggregation of NiO particles during the catalytic gasification process. A temperature of 800 °C is suitable for preventing coke deposition on the catalyst surface. However, this temperature is rather high and might possibly cause catalyst deactivation by Ni sintering after repeated use in the gasification process [38].

4. Conclusions

In this work, Ni-Mg-Al-Ca catalysts with different Ca content and calcination temperature were synthesized to enhance the in situ CO_2 absorption and increased hydrogen production from the pyrolysis-gasification of a mixture of wood sawdust and polypropylene.

By increasing the Ca content in the catalyst, hydrogen yield was improved to 33.2 mol H_2 g^{-1} Ni in the presence of the 750-Ca4 catalyst since the water-gas shift reaction was enhanced by in situ CO_2 absorption. In addition, lower calcination temperature was prefered for hydrogen production due to the presence of reactive CaO in the catalyst, resulting in the highest hydrogen yield of 39.6 mol H_2 g^{-1} Ni using the catalyst produced at a lower calicination temperature (500 °C (500-Ca4)).

TPO, TGA-FTIR, and SEM analyses of reacted catalysts revealed that Ca introduction in the Ni-Mg-Al catalyst prevented depositition of filamentous carbons on the catalyst surface. TEM-EDX analysis indicated that athe metals were well dispersed in the catalyst after the pyrolysis-gasification experiments. In addition, NiO particles after gasification were about 20 to 30 nm in size, which suggested that Ca introduction prevents aggregation of NiO particles during the catalytic gasification process.

Acknowledgements

Shogo Kumagai was partially supported by the Japan Society for the Promotion of Science (JSPS) (Grant-in-Aid for JSPS Fellows, 24-4996), the Ministry of Education, Culture, Sports, Science and Technology (MEXT) of the Japanese Goverment (Grant-in-Aid for Scientific Research (A), 25241022). Also, Jon Alvarez thanks The Basque Government for his research training grant (BFI2010-206) and the Ministry of Science and Education of the Spanish Government (Project CTQ2010-16133).

REFERENCES

1. BP BP Statistical Review of World Energy June 2013. http://www.bp.com/content/dam/bp/pdf/statistical-review/statistical_review_of_world_energy_2013.pdf (June 14),

2. A.F. Kirkels, G.P.J. Verbong, Renewable and Sustainable Energy Reviews 15 (2011) 15, 471.

3. Plastics Europe: Plastics-the Facts 2012. http://www.plasticseurope.org/cust/documentrequest.aspx?DocID=54693 (7 June 2013),

4. N. Gao, A. Li, C. Quan, F. Gao, F., International Journal of Hydrogen Energy 33 (2008), 5430.

5. C. Wu, Z. Wang, J. Huang, P.T. Williams, P. T. Fuel 106 (2013), 697.

6. S. Luo, B. Xiao, Z. Hu, S. Liu, X. Guo, M. He, International Journal of Hydrogen Energy 34 (2009), 2191.

7. K. Wang, W.S. Li, X.P. Zhou, Journal of Molecular Catalysis A: Chemical 283 (2008), 153.

8. A. Erkiaga, G. Lopez, M. Amutio, J. Bilbao, M. Olazar, Fuel 109 (2013), 461.

9. S. Zhang, K. Yoshikawa, H. Nakagome, T. Nakagome, Journal of Material Cycles and Waste Management, 14 (2012), 294.

10. S. Zhang, K. Yoshikawa, H. Nakagome, T. Kamo. Applied Energy, 101 (2013), 815.

11. J.M.N. van Kasteren. Journal of Material Cycles and Waste Management, 8, (2006), 95.

12. M. Brebu, S. Ucar, J.C. Vasile, Fuel, 89 (2010), 1911.

13. W.W. Liu, C.W. Hu, Y. Yang, D.M. Tong, L.F. Zhu, R.N. Zhang, B.H. Zhao. Applied Catalysis B: Environmental, 129 (2013), 202.

14. A. Demirbas, Energy Conversion and Management, 43 (2002), 897.

15. R. Muangrat, J.A. Onwudili, P.T. Williams, Applied Catalysis B: Environmental 100 (2010), 440.

16. W. Tongamp, Q. Zhang, F. Saito, International Journal of Hydrogen Energy 33 (2008), 4097.

17. B.S. Huang, H.Y. Chen, K.H. Chuang, R.X. Yang, M.Y. Wey, International Journal of Hydrogen Energy 37 (2012), 6511.

18. M. Asadullah, S.I. Ito, K. Kunimori, M. Yamada, K. Tomishige, Environmental Science and Technology, 36 (2002), 4476.

19. J.A. Onwudili, P.T. Williams, Applied Catalysis B: Environmental, 132 (2013), 70.

20. S. Czernik, R.J. French, Energy and Fuels, 20 (2006), 754.

21. G. Ruoppolo, P. Ammendola, R. Chirone, F. Miccio, Waste Management, 32 (2012), 724.

22. C. Wu, P.T. Williams, P. T., Applied Catalysis B: Environmental 90, (2009), 90, 147.

23. L. Garcia, A. Benedicto, E. Romeo, M.L. Salvador, J. Arauzo, R. Bilbao, R., Energy and Fuels, 16 (2002), 1222.

24. C. Wu, Z. Wang, V. Dupont, J. Huang, P.T. Williams, Journal of Analytical and Applied Pyrolysis 99, (2013), 143.

25. C. Wu, P.T. Williams, P. T. Fuel, 89 (2010), 1435.

26. M.A. Nahil, X. Wang, C. Wu, H. Yang, H. Chen, P.T. Williams, RSC Advances, 3 (2013), 5583.

27. D. Alvarez, J.C. Abanades, Energy and Fuels, 19 (2005), 270.

28. V. Manovic, E.J. Anthony, Environmental Science and Technology, 42 (2008), 4170.

29. R.H. Borgwardt. Chemical Engineering Science, 44, (1989), 53.

30. A.I. Lysikov, A.N. Salanov, A.G. Okunev, Industrial & Engineering Chemistry Research

46 (2007), 4633.

31. C. Wu, P.T. Williams, Applied Catalysis B: Environmental 87, (2009), 152.

32. C. Zhou, T. Stuermer, R. Gunarathne, W. Yang, W. Blasiak, Fuel, 122 (2014), 36.

33. C. Wu, P.T. Williams, P. T. Fuel, 89 (2010), 3022.

34. C. Wu, L. Wang, P.T. Williams, J. Shi, J. Huang, Applied Catalysis B: Environmental 108, (2011), 6.

35. C. Wu, P.T. Williams. Applied Catalysis B: Environmental 96 (2010), 198.

36. P. Wang, E. Tanabe, K. Ito, J. Jia, H. Morioka, T. Shishido, K. Takehira, K. Applied Catalysis A: General, 231 (2002), 35.

37. D.W. Mckee, Fuel, 59, (1980), 308.

38. A. Remiro, B. Valle, A.T. Aguayo, J. Bilbao, A.G. Gayubo, Fuel Processing Technology, 115 (2013), 222.

39. M. Inaba, K. Murata, M. Saito, I. Takahara, Energy and Fuels, 20, (2006), 432.

Table 1.

Proximate and ultimate analysis of the wood sawdust.

Proximate analysis*/wt%			
Moisture	Volatile	Fixed carbon	Ash
6.4	74.8	18.3	1.2
Ultimate analysis/wt%			
Carbon	Hydrogen	Nitrogen	Oxygen**
47.1	5.9	0.1	46.9

*On wet basis

**Calculated by mass difference

Table 2.

Abbreviations and preparation conditions of the catalysts at different metal composition and calcination temperature.

Abbreviation	Calcination temperature /°C	Molar ratio of metals Ni:Mg:Al:Ca	Ni content /wt%	Ca content /wt%
750-Ca0	750	1:1:1:0	35.4	0.0
750-Ca2	750	1:1:1:2	21.1	28.8
750-Ca4	750	1:1:1:4	15.0	41.1
500-Ca2	500	1:1:1:2	21.1	28.8
500-Ca4	500	1:1:1:4	15.0	41.1

Table 3.

Mass balance of the decomposition products in the presence of different catalysts.

Calcination Temp.		750 ºC			500 ºC	
Ni:Mg:Al:Ca ratio	No Cat.	1:1:1:0	1:1:1:2	1:1:1:4	1:1:1:2	1:1:1:4
Mass balance based on the sample + water/wt%						
Gas	19.5	38.1	35.1	32.6	37.3	33.7
Liquid	72.0	55.5	55.5	54.8	51.3	55.2
Char	6.4	7.1	7.2	7.5	7.4	7.1
Mass Balance (wt%)	97.9	100.7	97.8	94.9	96.0	95.9
Mass balance based on the sample/wt%						
Gas	52.9	96.9	89.0	79.7	90.9	83.4
Char	17.2	18.0	18.2	18.4	17.9	17.6

Figure Captions

Fig. 1. Schematic diagram of the experimental system.

Fig. 2. Hydrogen yield in relation to sample and nickel weight in the presence of different catalysts.

Fig. 3. Gas composition and H_2/CO ratio in the presence of different catalyst.

Fig. 4. Pyrolysis/hydrogen production scheme from wood sawdust (WS)/polypropylene (PP) in the presence of Ni-Mg-Al-Ca catalyst.

Fig. 5. TPO thermograms of the reacted catalysts obtained after wood sawdust/polypropylene gasification.

Fig. 6. TGA-FTIR spectrogram of the reacted 750-Ca4 obtained after wood sawdust/polypropylene gasification.

Fig. 7. SEM images of fresh and reacted catalysts. (a) Fresh 750-Ca0, (b) Reacted 750-Ca0, (c) Fresh 750-Ca2, (d) Reacted 750-Ca2, (e) Fresh 750-Ca4, (f) Reacted 750-Ca4, (g) Fresh 500-Ca2, (h) Reacted 500-Ca2, (i) Fresh 500-Ca4, and (j) Reacted 500-Ca4.

Fig. 8. TEM images of the reacted catalysts. (a) 750-Ca2 (250 kX), (b) 750-Ca2 (1000 kX), (c) 500-Ca4 (250 kX), and (d) 500-Ca4 (1000 kX).

Fig. 9. TEM image, elemental mapping, and EDX spectrum of the reacted 750-Ca2 catalyst.

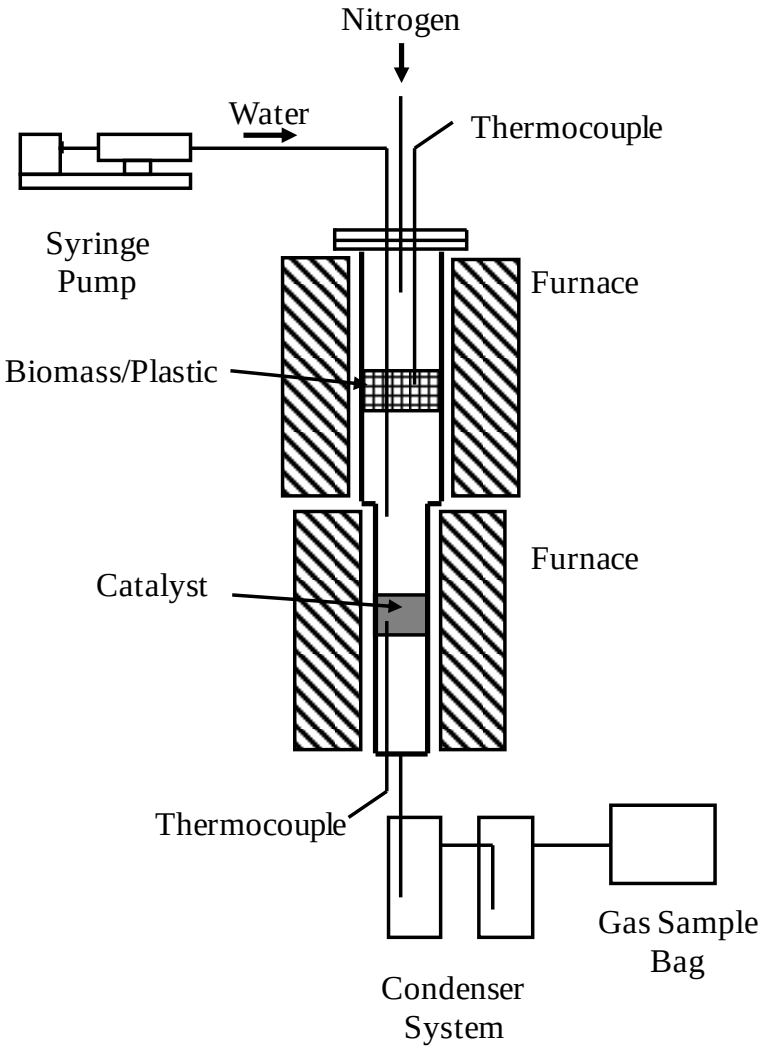
Nitrogen
Water
Thermocouple
Syringe
Pump
Furnace
Biomass/Plastic
Furnace
Catalyst
Thermocouple
Gas Sample
Bag
Condenser
System

Figure 1

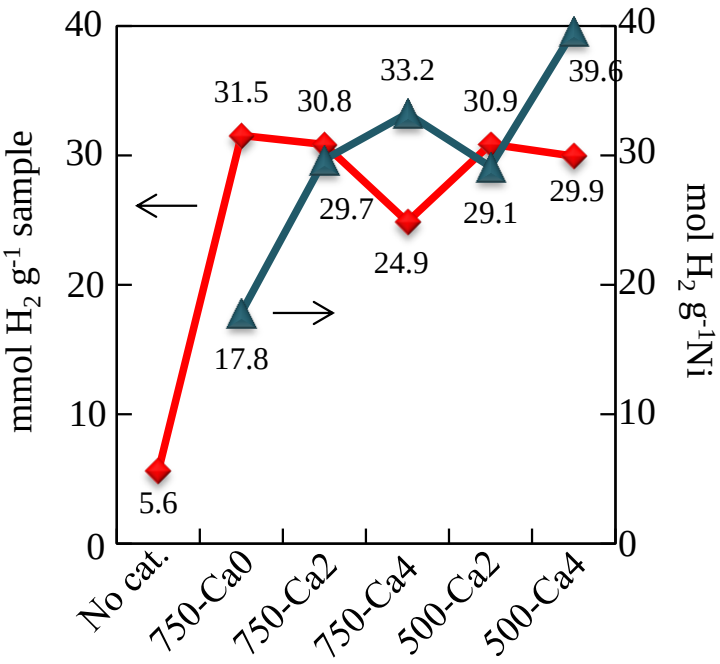
40
30
20
10
0
mmol H2 g-1 sample
mol H2 g-1Ni
31.5
30.8
33.2
30.9
39.6
29.7
29.1
29.9
24.9
17.8
5.6
No cat.
750-Ca0
750-Ca2
750-Ca4
500-Ca2
500-Ca4

Figure 2

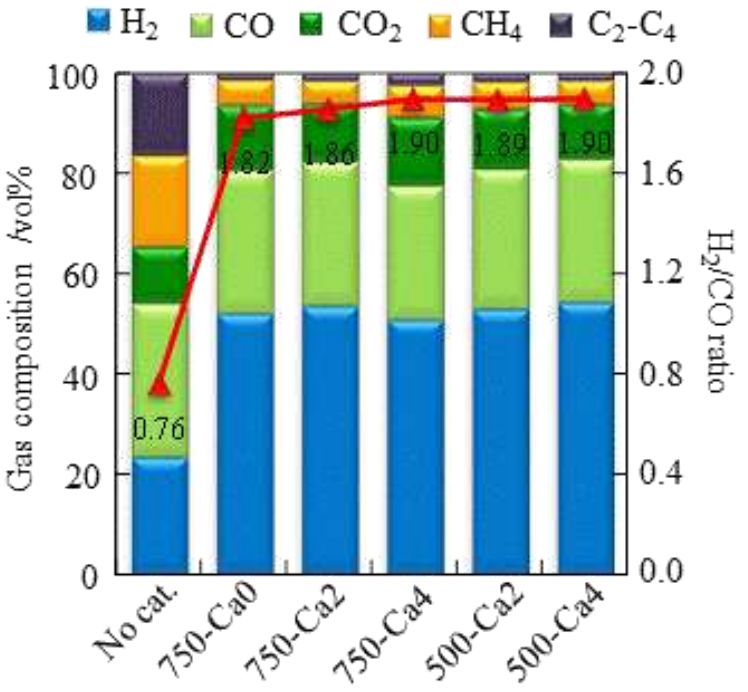
H2
CO
CO2
CH4
C2-C4
Gas composition /vol%
H2/CO ratio
100
80
60
40
20
0
2.0
1.6
1.2
0.8
0.4
0.0
0.76
1.82
1.86
1.90
1.89
1.90
No cat.
750-Ca0
750-Ca2
750-Ca4
500-Ca2
500-Ca4

Figure 3

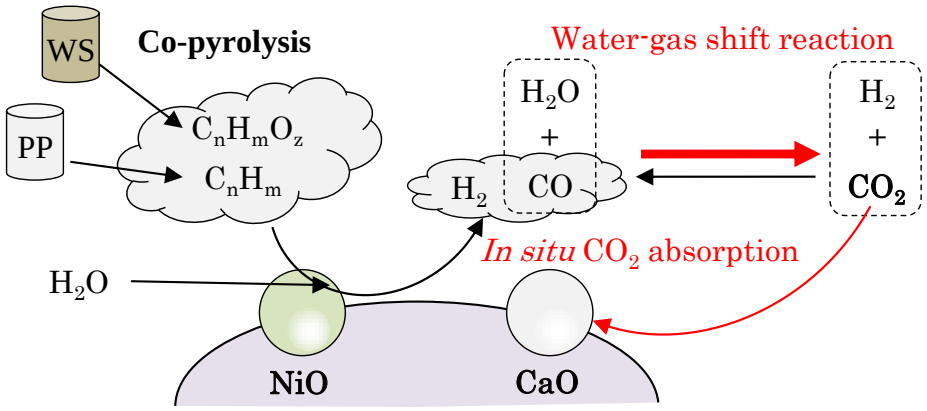
WS
Co-pyrolysis
PP
$C_nH_mO_z$
C_nH_m
H_2O
H_2O
+
H_2
CO
Water-gas shift reaction
H_2
+
CO_2
In situ CO_2 absorption
NiO
CaO

Figure 4

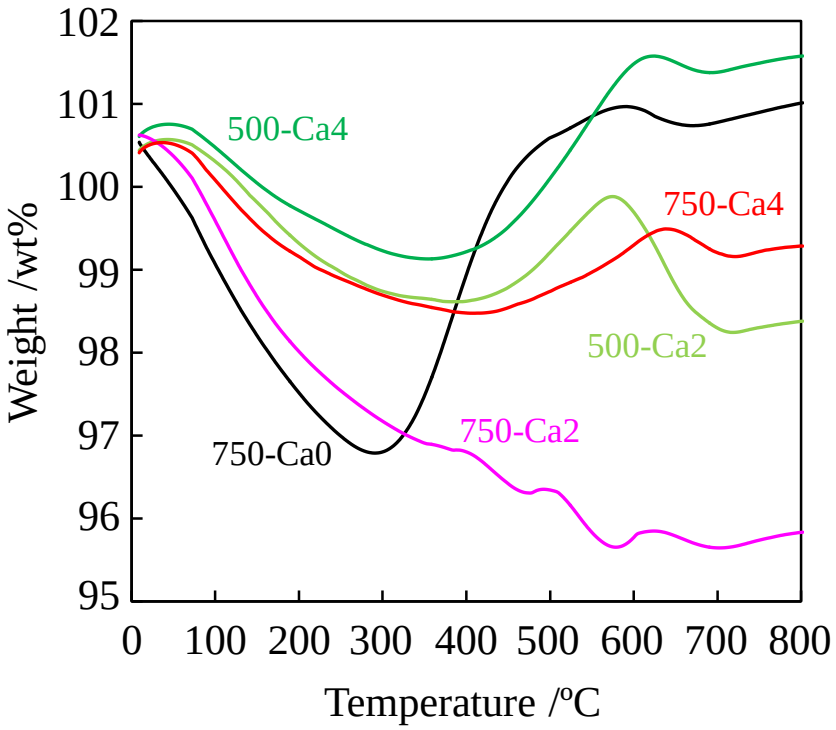
102
101
100
99
98
97
96
95
Weight /wt%
0
100
200
300
400
500
600
700
800
Temperature /ºC
500-Ca4
750-Ca4
500-Ca2
750-Ca2
750-Ca0

Figure 5

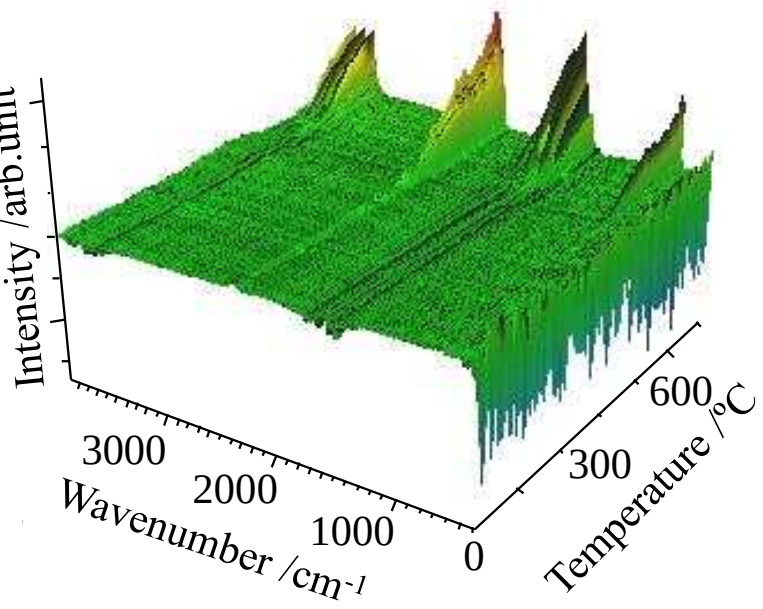
Intensity /arb.unit
3000
2000
1000
0
Wavenumber /cm-1
300
600
Temperature /°C

Figure 6

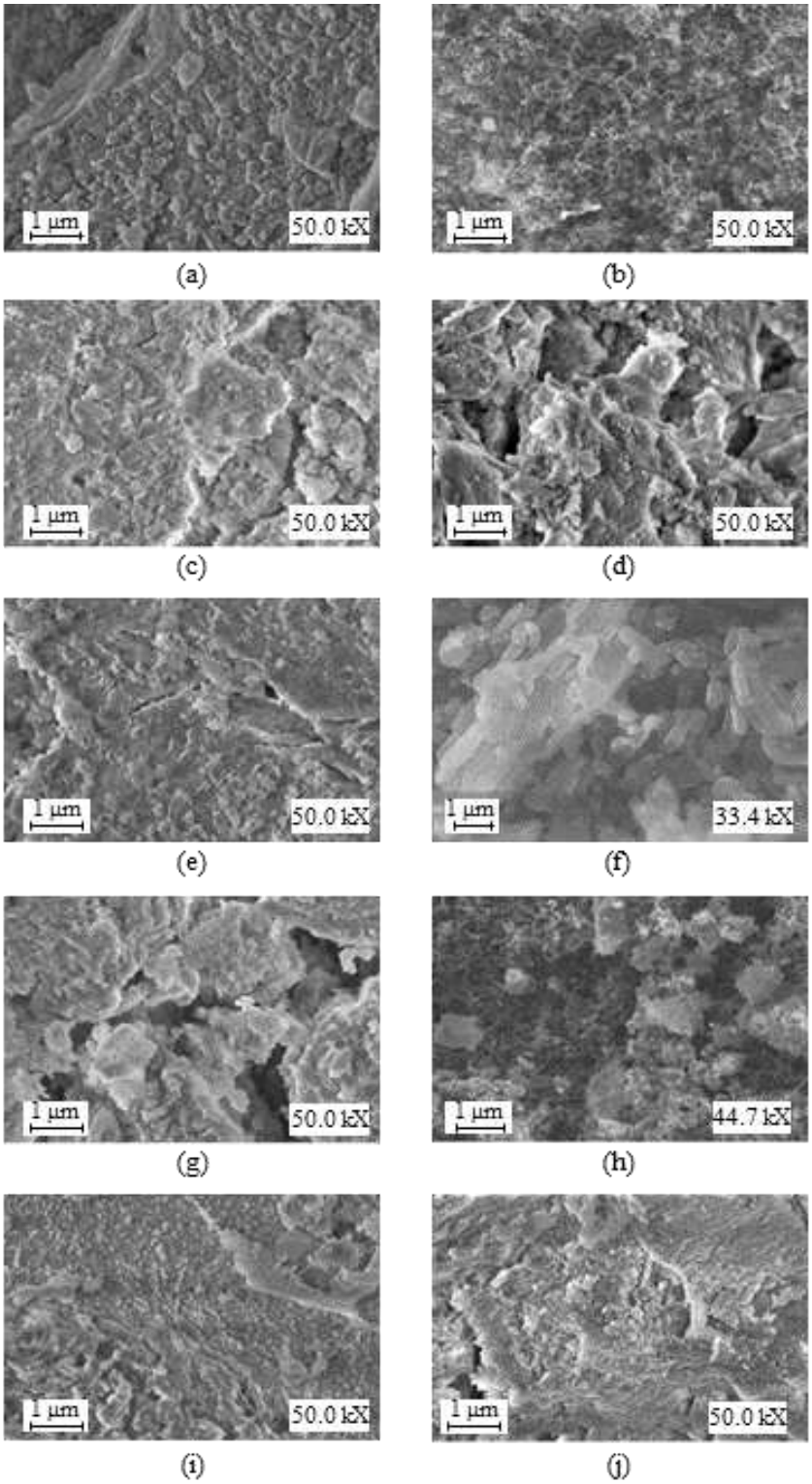
1 µm
50.0 kX
(a)
1 µm
50.0 kX
(b)
1 µm
50.0 kX
(c)
1 µm
50.0 kX
(d)
1 µm
50.0 kX
(e)
1 µm
33.4 kX
(f)
1 µm
50.0 kX
(g)
1 µm
44.7 kX
(h)
1 µm
50.0 kX
(i)
1 µm
50.0 kX
(j)

Figure 7

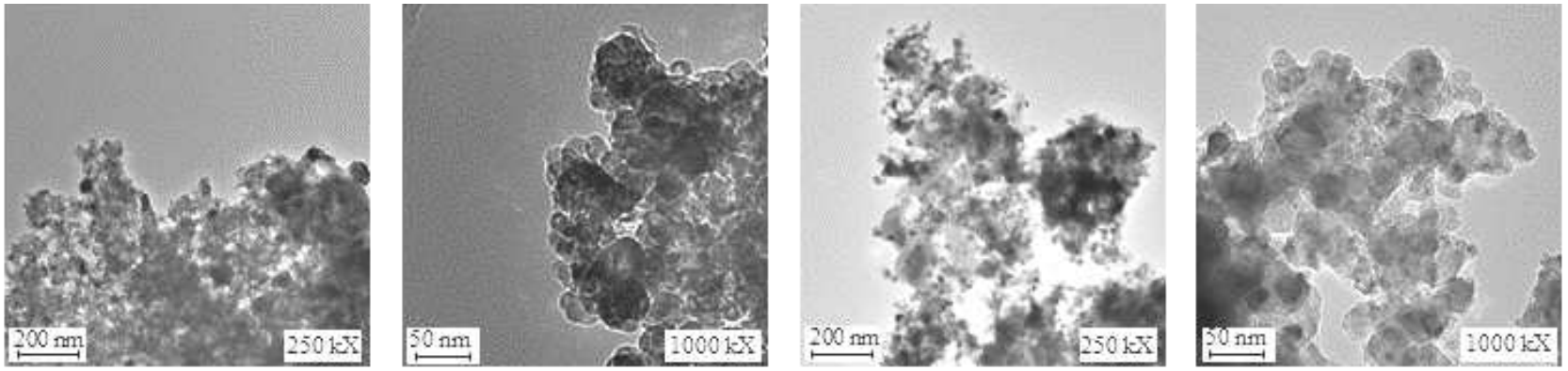

Figure 8

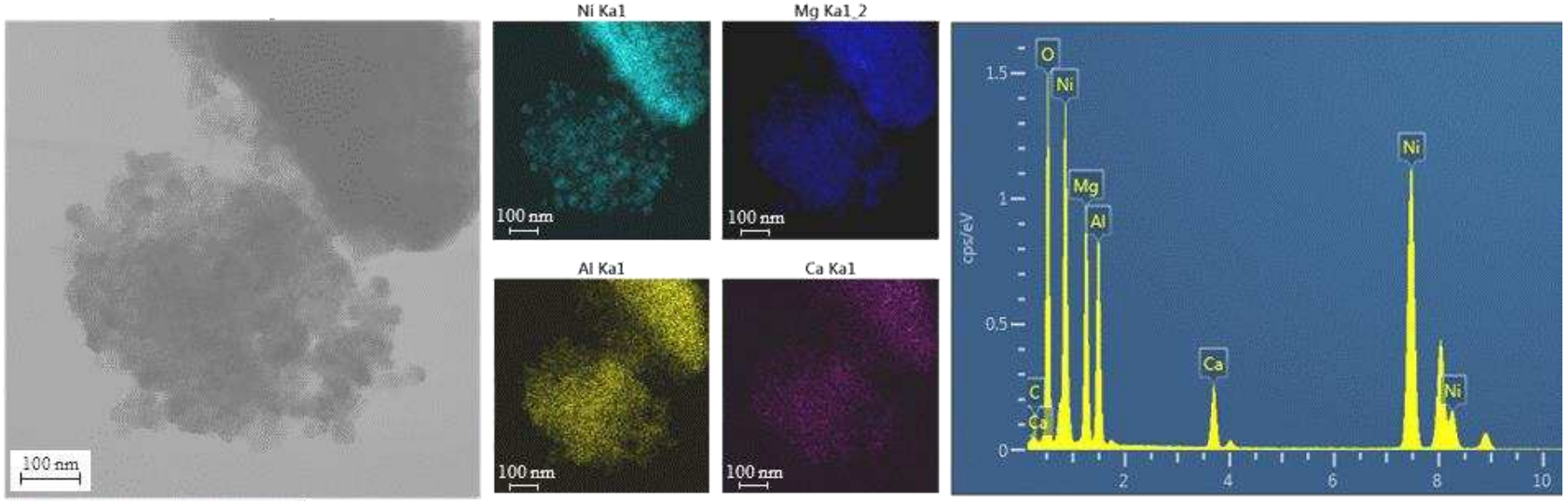
100 nm
Ni Ka1
100 nm
Mg Ka1_2
100 nm
Al Ka1
100 nm
Ca Ka1
100 nm
cps/eV
O
Ni
Mg
Al
Ca
Ni
Ni
C
Ca
1.5
1
0.5
0
2
4
6
8
10

Figure 9